JOURNAL OF THEORETICAL
AND APPLIED MECHANICS
https://doi.org/10.15632/jtam-pl/205163
ONLINE FIRST

EXPLOITATION PARAMETERS OF DEFORMED HIGH-STRENGTH STEEL ASSESSED BY THE BARKHAUSEN NOISE METHOD

Katarzyna MAKOWSKA[1*], Tadeusz SZYMCZAK[2], Zbigniew L. KOWALEWSKI[3]

[1] *Faculty of Mechatronics, Armament and Aerospace, Military University of Technology, Warsaw, Poland*
[2] *Department of Vehicle Type-Approval & Testing, Motor Transport Institute, Warsaw, Poland*
[3] *Department of Experimental Mechanics, Institute of Fundamental Technological Research, Polish Academy of Sciences, Warsaw, Poland*

*corresponding author, *katarzyna.makowska@wat.edu.pl*

The elastic limit, yield point, strain hardening component, and strength coefficient of martensitic steel were determined after monotonic tensile loading. The monotonic tension test of 41Cr4 steel was conducted for selected values of deformation. The specimen was unloaded after each pre-strain. The parameters from destructive tests were compared with those from the Barkhausen noise (BN) method obtained. It turned out that the magnetic Barkhausen effect can be helpful in the diagnostics of structural steel components and devices. Linear relationships between the elastic limit/yield point and parameters coming from the rms voltage of Barkhausen noise envelope were found.

Keywords: yield point; elastic limit; strain hardening component; strength coefficient; magnetic Barkhausen noise.

1. Introduction

Assessment of mechanical properties is crucial from an engineering point of view especially in situations requiring a high level of operational safety of responsible structures. The elastic limit and yield point are the basic mechanical properties that affect limits of material behaviour during its exploitation. On the other hand, the strain hardening exponent (n) and strength coefficient (K) are usually required for the accurate design analysis of components and engineering structures (Li *et al.*, 2019). It is well known that a long-term usage of objects connected even with a small increase in monotonic load generates a difference in working conditions. An unexpected load may produce additional deformation of materials and significantly affect the safety of structures. Among many types of deformation, the plastic flow may be treated as a major reason for components failure in several branches of industry (Kashefi *et al.*, 2023). As a consequence, the main objective of this work is to propose an effective method for determining the variation in mechanical properties using a non-destructive method based on the Barkhausen noise (BN) effect applied after tensile monotonic loading. This technique is proposed instead of destructive tests that require cutting parts from the structure to prepare specimens for subsequent testing. The BN offers an attractive tool for detecting a degree of deformation within the ferromagnetic materials (Kleber & Vincent, 2004). It enables the testing of materials in four stages: perfectly

The publication has been funded by the Polish Ministry of Science and Higher Education under the Excellent Science II programme "Support for scientific conferences".
The content of this article was presented during the 40th Danubia-Adria Symposium on Advances in Experimental Mechanics, Gdańsk, Poland, September 24–27, 2024.

elastic, micro-yielded, macro-yielded, and after progressive plastic deformation (Vaidyanathan *et al.*, 1999). Therefore, it can be suitable to evaluate a condition of the structural components and devices in service and help to find places where potential cracks may occur.

2. Theoretical background

The BN method is based on the magnetic Barkhausen effect. The BN effect represents the irreversible movement of domain walls during a magnetization cycle (Cullity & Graham, 2009). The movements appear discontinuously, because the domain walls are temporarily pinned by microstructural barriers, such as dislocation tangles, precipitations, grain boundaries, and voids, and subsequently, they are released abruptly in the changing magnetic field (Cullity & Graham, 2009). The stepwise breakaway of domain walls from the obstacles changes the magnetization state locally. Then, local changes in magnetization induce pulsed eddy currents, which activate electrical voltage pulses that may be detected by a searching coil or magnetic receiving head (Cullity & Graham, 2009). Stupakov *et al.* (2007) found that BN is sensitive to dislocation tangles introduced by plastic deformation. This also means that BN can also be sensitive to the applied stress. Such a phenomenon was explained by (Kleber & Vincent, 2004) at the level of the crystallographic network using pure iron as an example.

In the case of unloaded material, the magnetic moments of domains are oriented along the easy direction of magnetization. In the case of iron, the [100] represents the easy direction of magnetization. A tensile stress causes a change in the direction of easy magnetization. Both the magnetic domains and magnetic moments become parallel to the axis of stress action – they are locally privileged and grow at the expense of others. The privileging of domain walls results from the equation defining the magnetoelastic energy

$$E_m = -1.5 \cdot \lambda_s \cdot \cos^2(\phi), \tag{2.1}$$

where E_m – magnetoelastic energy of isotropic material; λ_s – magnetostriction constant for isotropic material $\lambda_{100} = \lambda_{111} = \lambda_s$; ϕ – the angle between the direction of stress $\boldsymbol{\sigma}$ and the direction of the vector local magnetization $\mathbf{J}_s$.

Since either the tensile stress or magnetostriction constants for iron are positive, their multiplication product also takes the positive value. The magnetoelastic energy reaches a minimum when the moments of magnetic domains are arranged to each other in a parallel way. As a consequence, the angle between the direction of local magnetization vector $\mathbf{J}_s$ and the direction of stress $\boldsymbol{\sigma}$ equals 0.

The Barkhausen signal decreases due to the appearance of the induced anisotropy of the material after exceeding the critical stress value. The sign of the magnetostriction constant for the iron changes from positive to negative for the magnetic field strength of about $16\,\mathrm{kAm}^{-1}$ (Cullity & Graham, 2009). Simultaneously, the easy magnetization direction of iron crystal changes from [100] to [111] (Kleber & Vincent, 2004). Magnetic domain walls are arranged lengthwise in the [111] easy magnetization direction, differently from the stress direction (Anglada-Rivera *et al.*, 2001). The influence of external tensile stress on the changes in the domain structure and in the BN level was also discussed in (Anglada-Rivera *et al.*, 2001). Moreover, the effect of compressive stress on domain walls behaviour was studied in (Stewart *et al.*, 2004).

In the case of compressive stress, the domains of the materials with a positive magnetostriction contrast and having their magnetic moments perpendicular to the axis of the applied stress become energetically favourable (Kleber & Vincent, 2004). Then, the magnetoelastic energy of the ferromagnetic material achieves a minimum. As a consequence, the angle between the direction of local magnetization vector $\mathbf{J}_s$ and the direction of stress $\boldsymbol{\sigma}$ equals 90°. The 90° domain walls enlarge at the expense of other domains (Kleber & Vincent, 2004). In this case, the BN signal decreases. Stupakov *et al.* (2007) studied CSN12013 low-carbon steel ($C = 0.03\,\%$) subjected to plastic deformation up to 23 %. It was found that the effective stress of the Barkhausen

emission initially increases (up to approximately 2.5 %) with an increase in plastic deformation and then decreases. Similar results were found in (Piotrowski *et al.*, 2009) for CSN12021 steel tested up to 18.2 %. The highest BN amplitude was obtained for the specimen deformed to 1.9 %.

The problem of elastic tensile or compressive stresses effect on the magnetic BN is well recognized. However, the correlation between BN and plastic deformation is still a matter of intense investigation. From the microstructural point of view, the dislocations create different consequences during plastic deformation. In the early stage of the deformation process, they are distributed randomly and independently (Kashefi *et al.*, 2023). In the further stages of the deformation process, dislocations form sub-grains consisting of dislocation cells of hard density in the case of cell walls and lower density for the cell interior (Kashefi *et al.*, 2023). The soft and hard dislocation regions are responsible for a formation of the residual internal stress of type II after unloading of the previously plastically deformed material (Hong *et al.*, 2018). Dislocation tangles and cells interact with domain walls as the pinning sites and affect the BN signal (Cullity & Graham 2009). As a result, a change in the magnetic anisotropy may occur (Cullity & Graham 2009), and therefore, a change in the BN level can be observed.

According to the available literature, plastic deformation affects significantly the mechanical properties of materials. This research aims to find an answer to the questions how large changes in mechanical parameters are, and whether they can be determined using the BN technique. The elastic limit, yield point, strain hardening coefficient and strength coefficient were determined based on the relationships between parameters coming from monotonic tensile tests and the BN method. To date, the BN analysis has not been performed on a material subjected to repeated plastic deformation. The experiment demonstrates the possibilities of estimating material properties in worn-out structural parts involved in service downtime.

3. Material and experimental procedure

41Cr4 steel was selected for tests due to its wide application in automotive components, e.g., crankshafts, steering components, gears, front axle bearings. The steel is still an attractive structural material due to its high strength and qualified toughness (Celtik *et al.*, 2023). However, as of now, there are still some areas of knowledge requiring further thorough studies devoted to an influence of stress on mechanical parameters of plastically deformed zones (Romanowicz *et al.*, 2020).

The experimental procedure contained two main steps: monotonic tensile tests up to the selected values of deformation and the BN measurements. Mechanical tests were carried out at room temperature using flat specimens on the 8802 Instron servo-hydraulic testing machine. Strain was measured by means of the 2630 Instron uni-axial extensometer. The width, gauge length and thickness of the specimen were 10 mm, 25 mm, and 3 mm, respectively. The total length of the specimen was 174.5 mm (Fig. 1). The specimens were loaded monotonically under strain control with loading velocity of 0.005 mm/mm. The following levels of deformation were applied: 1 %, 2 %, 3 %, 4 %, 6 %, 8 %, 10 %, 12 %, 14 %. After each pre-strain, the specimen was unloaded. The yield point (YP), elastic limit (EL), strain hardening exponent (n), and strength coefficient (K) were determined for each loading process.

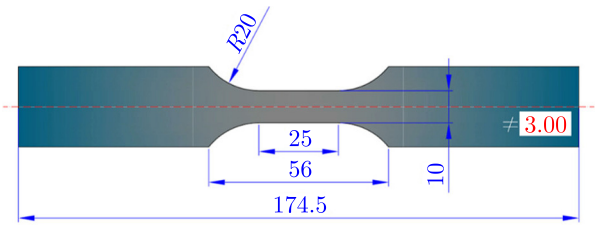

Fig. 1. Dimensions of specimen used in the experiment.

The BN measurements were performed using an MEB-4C defectoscope with a head consisting of a U-shaped core of electromagnets wrapped in the wound excitation coil. The pick-up coil was built into the sensor. In the pick-up coil, a voltage signal was induced. A triangular waveform was used. The fast-variable component was separated using a high-pass filter $f = (0\text{–}500)$ Hz. The analysis of this component provided information on the strain level degree of the steel tested. The envelopes of magnetic BN were calculated as rms value U_b according to the following equation (Makowska *et al.*, 2024):

$$U_b = \sqrt{\frac{1}{\tau}\int_0^{\tau} U_{tb1}^2(t)\,\mathrm{d}t}, \tag{3.1}$$

where U_b – root mean square (rms) of the coil output voltage [V], U_{tb1} – fast-variable component defining voltage separated using the high-pass filter from the induced voltage in the pick-up coil [V], τ – integration time [s].

Then, the amplitude of BN ($U_{b\,pp}$), defined as the voltage difference between the maximum peak value of the magnetic BN (U_b) and the background noise (U_{tb}), was determined. Moreover, the integral of the half-period voltage signal of MBN was calculated (Makowska *et al.*, 2024):

$$\mathrm{Int}(U_b) = \int_{-Ug\,\max}^{+Ug\,\max} U_{sb}\,\mathrm{d}U_g, \tag{3.2}$$

where U_{sb} – rms of the Barkhausen emission voltage after correction with respect to the background noise [V], U_{tb} – rms of the background voltage [V], U_g – generator voltage [V].

The last step of the experimental programme was to find relationships between such mechanical parameters as elastic stress, yield point, maximal axis stress, stain hardening coefficient and parameters coming from rms of the BN envelope.

4. Results and analysis

The 41Cr4 steel stress-strain curves after various pre-strains are presented in Fig. 2. Important differences in tensile curves were found in the range from 0 % to 1 %. It was observed that the yield point and elastic limit increased with the pre-strain level (Fig. 3).

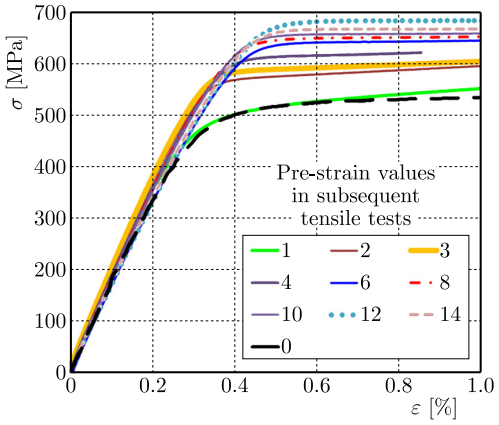

Fig. 2. Comparison of the tensile curve in the initial range of deformation for 41Cr4 in the as-received state to characteristics determined after the subsequent 9 steps of the loading-unloading process.

The greatest strengthening was achieved for an initial deformation of 0.12 mm/mm. The maximum value of the yield point was 690 MPa for the pre-strain level of 12 %, whereas the maximum

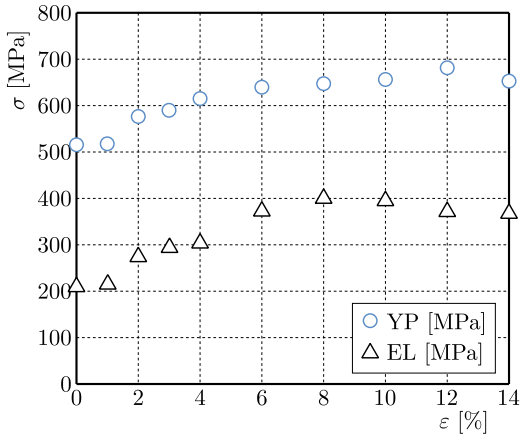

Fig. 3. Elastic limit (EL) and yield point (YP) versus total axial strain achieved during subsequent loading steps.

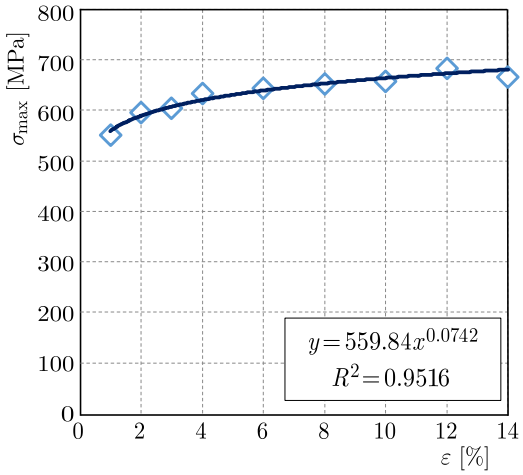

Fig. 4. Maximum value of axial stress versus total axial strain achieved during subsequent loading steps.

value of the elastic limit was 400 MPa for pre-strain of 8 % (Fig. 3). It means that 41Cr4 steel is sensitive to prior deformation and its mechanical parameters after loading to achieve 12 % pre-strain were almost 200 MPa higher than those for the same material in the as-received state obtained. The hardening was stabilized for the higher deformation reflected by similar values of the yield point and elastic limit. One can conclude that the pre-straining created almost a perfect elasto-plastic material with a little hardening effect. Also variations of the strain hardening exponent that was equal almost to zero for the highest strain level confirm such behaviour (Fig. 5). As is shown in Fig. 4, the maxiumum value of axial stress versus total axial strain increased

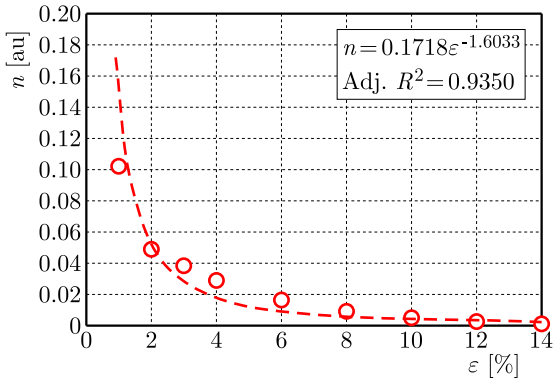

Fig. 5. Strain hardening exponents versus total axial strain achieved during subsequent loading steps.

during subsequent loading steps. Changes in the strength coefficient decreased asymptotically up to the constant level with an increase in the total axial strain (Fig. 6). The power-law work hardening equations for various values of the total strain are presented in Table 1. The true stress-plastic strain relationship is described by the equation $\sigma = K\varepsilon^n$ (Li *et al.*, 2019), where σ is the true stress, ε is the true plastic strain, K is the strength coefficient, and n is the strain hardening coefficient.

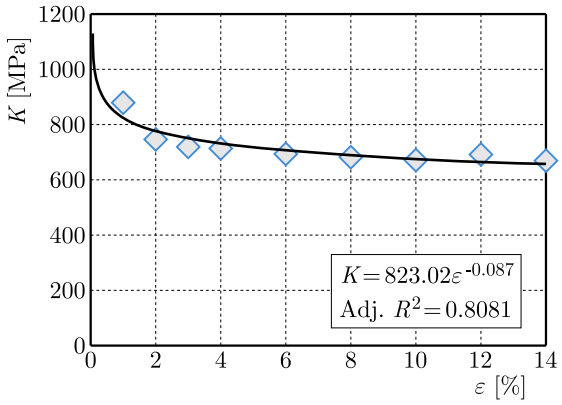

Fig. 6. Changes in strength coefficient versus total axial strain achieved during subsequent loading steps.

Table 1. Power-law work hardening equations for the total axial strain achieved during subsequent loading steps for 41Cr4 steel.

Total axial strain	Power-law hardening equation
1 %	$\sigma = 882.41\varepsilon^{0.1018}$
2 %	$\sigma = 743.44\varepsilon^{0.849}$
3 %	$\sigma = 719.37\varepsilon^{0.0383}$
4 %	$\sigma = 713.05\varepsilon^{0.0291}$
6 %	$\sigma = 695.29\varepsilon^{0.0165}$
8 %	$\sigma = 679.31\varepsilon^{0.0091}$
10 %	$\sigma = 673.69\varepsilon^{0.0052}$
12 %	$\sigma = 690.86\varepsilon^{0.0025}$
14 %	$\sigma = 669.28\varepsilon^{0.001}$

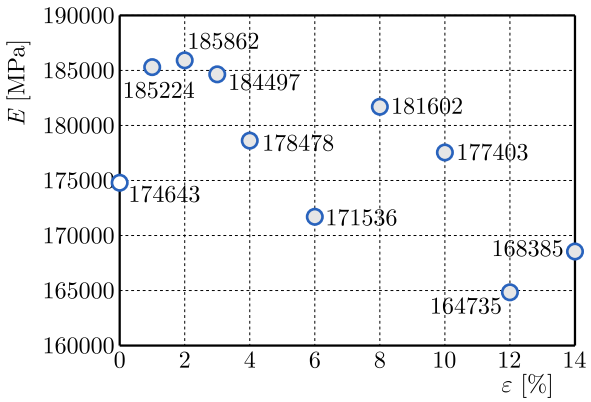

Fig. 7. Young's modulus versus total axial strain achieved during subsequent loading steps.

The effect of plastic deformation was also observed using the BN non-destructive method. It was found that the rms BN envelopes are sensitive to the pre-strain level (Fig. 9). The amplitude (Fig. 10) and the integral of BN (Fig. 11) decrease up to 6 % of plastic pre-strain. For its higher levels, both parameters take the constant value. For a better interpretation of the BN results,

the points representing subsequent levels of prior deformation were introduced on the tensile curve of 41Cr4 steel (Fig. 8).

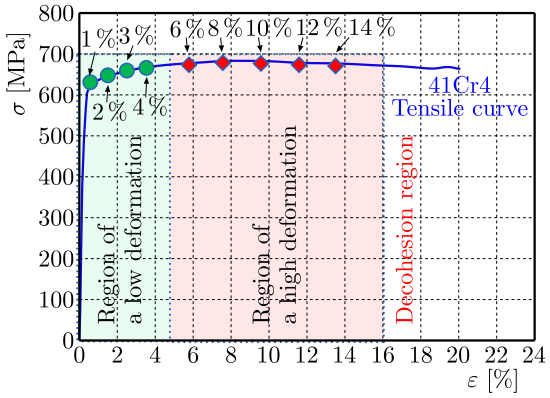

Fig. 8. Tensile curve of 41Cr4 steel with points illustrating the total strain values achieved during subsequent loading steps.

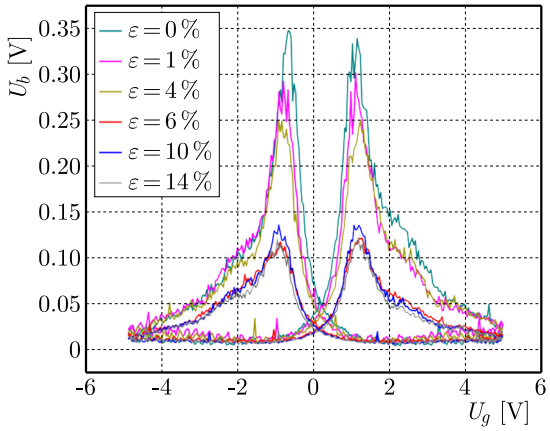

Fig. 9. Envelopes of rms BN before and after prior deformation.

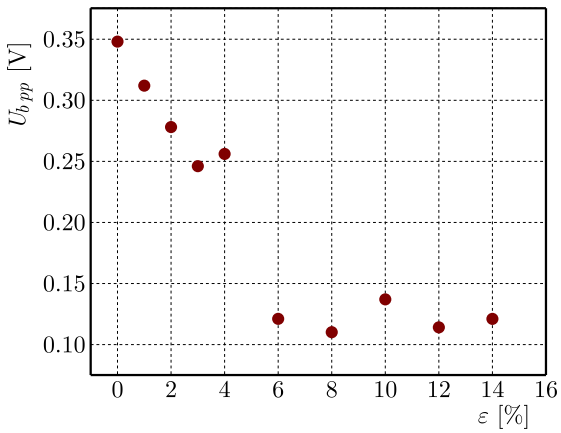

Fig. 10. Amplitude of rms BN envelopes versus total axial pre-str.

Figures 11 and 14 show that the BN is most sensitive in the elastic range of stress characteristic. In this case, the dislocation line length does not change significantly and the BN depends on changes in the crystal lattice. As a consequence, a rearrangement of the magnetic moments in magnetic domains through magnetoelastic energy takes place. In the elastic range, dislocations bow out and create a zig-zag segment structure. It indicates that the intergranular dislocation slip started before the initial plastic stage (Wang *et al.*, 2020). These are early

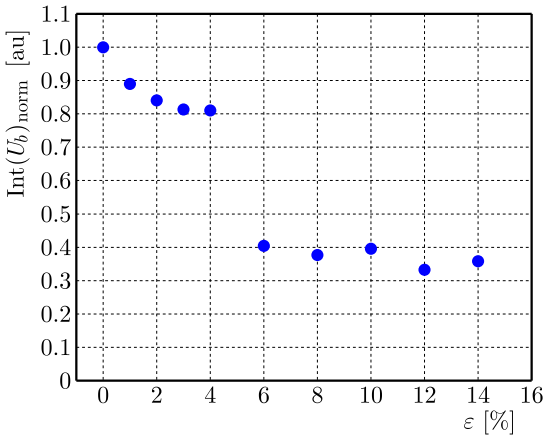

Fig. 11. Normalized Int(U_b) versus total axial pre-strain.

signs of plastic deformation also called micro-yielding. Generally, dislocations are likely to be generated first in the grain boundary regions during micro-yielding (Stefanita, 1999). As the grain slip process occurs partially, the plastic flow starts to appear in the material. The Barkhausen noise signal decreases with the plastic strain until the material becomes fully macro-yielded.

If the yield point is reached, then dislocations can be formed in the grain interior and the macroscopic yielding can occur by a massive generation of dislocations motion. In consequence, dislocation density becomes similar in boundary regions and inside the grain (Stefanita, 1999).

The dislocation tangles of high dislocation density create pinning sites during the further plastic deformation process. Forming dislocation configurations hinders the movement of the domain walls and the BN signal decreases.

This means that the Domain Walls (DWs) movements are hindered by defects of larger geometrical size (He *et al.*, 2019). According to (He *et al.*, 2019), magnetic domains are stuck between the micro-defects. Plastic deformation over 1 % introduced through the single-cycle loading process changes material isotropic orientation to the unique orientation of magnetic domains. Conversely, plastic deformation lower than 0.5 % and introduced by several loading processes leads to the cataclastic domain structures with weak orientation (He *et al.*, 2019).

When the specimen is stretched to 3 %, a dislocation density increases and distributes homogeneously. According to Mughrabi's composite model, the structure with dislocation-rich cell walls and dislocation-rich walls is created (Dannoshita *et al.*, 2023). Edge dislocations create dislocation cell walls, whereas screw dislocations are the main components of the cell interiors (Dannoshita *et al.*, 2023).

Dislocation tangles develop with plastic strain and dislocation lines intertwined with each other. Within the range of strain $\varepsilon = 10\,\%$–$14\,\%$, dislocation pile-up occurred and dislocation net structures consisted of high-density dislocation tangles developed (Wang *et al.*, 2020). Moreover, the formation of voids under tensile stress can be observed (Wang *et al.*, 2020). The voids are created in both regions of high dislocation density as well as the precipitated phase vicinity, and they serve as the demagnetization areas that contribute to the BN signal reduction.

An interesting feature can be observed by the analysis of Young's modulus variations due to subsequent steps of prior deformation. Studies of Young's modulus as a function of strain were repeatedly undertaken in (Roca *et al.*, 2014). A decrease in Young's modulus after plastic deformation was noticed in the low-carbon steel delivered in the form of sheets. It varied from 215 GPa, 200 GPa, 195 GPa for pre-strain of 0 %, 10 % and 15 %, respectively (Yamaguchi *et al.*, 1998). It was also observed that Young's modulus of the low-carbon steel sheet could be recovered to the value of undeformed sheet by subsequent annealing (Yamaguchi *et al.*, 1998). Researchers presumed that a decrease in Young's modulus came mainly from the microscopic debonding at the interface between inclusions or 2nd-phase particles and matrix (Yamaguchi *et al.*, 1998).

Similar tendency was obtained for a ductile iron by Berdin and HauŠild (2002). In this case, a debonding at the interface between graphite nodules and metallic matrix was responsible for Young's modulus lowering. In (Rutecka *et al.*, 2020), debonding between SiC particles and aluminium matrix was observed in the form of small microstructural discontinuities and cracks around SiC particles. It led to a decrease in Young's modulus with plastic deformation (Rutecka *et al.*, 2020). However, in the case of 41Cr4 steel tested in this research, Young's modulus seems to be insensitive to prior deformation (Fig. 7). From the microstructural point of view, Young's modulus values could be attributed to certain categories depending on the strain range. One can indicate the first range if $\varepsilon = 1\,\%$–$3\,\%$, the second one if $\varepsilon = 3\,\%$–$10\,\%$, and the third one if $\varepsilon = 10\,\%$–$14\,\%$. As it was mentioned earlier, the first range corresponds either to micro-yielding or macro-yielding where there are no significant material inhomogeneities, so E = 185 GPa–186 GPa. The second range represents an increase in inhomogenously distributed dislocations. Dislocations increase and interact with each other inside the crystal in the homogenous plastic region. A threshold of the slip process is increased by the hardening of the material. So, E = 172 GPa–182 GPa. In the third range ($\varepsilon = 10\,\%$–$14\,\%$), voids in the material occur near very high dislocation tangles. The steel structure becomes very inhomogeneous, so Young's modulus drops below 170 GPa (takes values between 165 GPa and 168 GPa). An influence of dislocation density on Young's modulus was discussed in (Benito *et al.*, 2005). The authors noticed that Young's modulus of pure iron decreased after plastic deformation from the original mean value of 210 GPa to 196 GPa at $\varepsilon = 0.060$. Next, a slight recovery occurred and Young's modulus increased to 198 GPa until the neck appeared at $\varepsilon = 0.100$ (Benito *et al.*, 2005). An explanation of such behaviour is based on Mott's model (Benito *et al.*, 2005). It was proposed that the assumed dislocations can bow out in their glide planes, giving an extra elastic strain, and thus, a decrease in Young's modulus. According to Mott's theory, the first steps of deformation in pure iron lower Young's modulus due to the dislocation density and the extra elastic strain increase (Benito *et al.*, 2005). Hence, when the cellular dislocation structure has formed during plastic deformation at higher strains (between $\varepsilon = 0.060$ and 0.080), the dislocations in cell interiors may give an extra elastic strain (Benito *et al.*, 2005). In the early stages of deformation, the cell structure is not able to develop, so the dislocation density in cell interiors is lower than that in the first deformation stage observed. It causes the slight recovery of Young's modulus measured at the strain ranges considered. Finally, for the higher strain values than $\varepsilon = 0.080$, no changes of dislocation density in cell interiors are observed and the values of Young's modulus are stabilized (Benito *et al.*, 2005).

The change in parameters coming from the BN envelope can be considered separately for low and high degrees of prior deformation. The linear relationship between the BN amplitude and pre-strain was found (Fig. 12). Exponential dependence was observed in the case of the BN integral and prior deformation (Fig. 14). However, both BN parameters are insensitive to higher levels of pre-strain (Fig. 13 and Fig. 15).

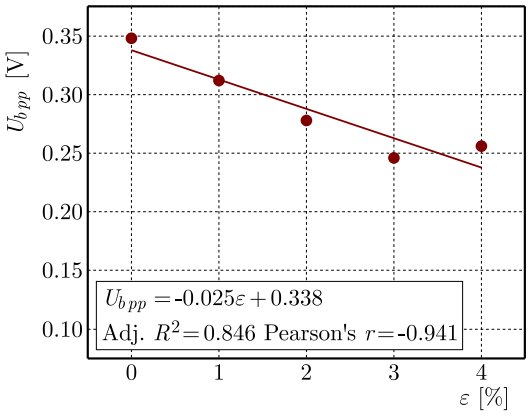

Fig. 12. Amplitude of rms BN envelopes versus low total axial pre-strain.

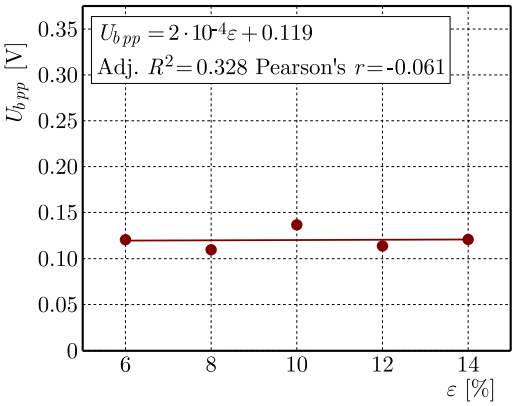

Fig. 13. Amplitude of rms BN envelopes versus high total axial pre-strain.

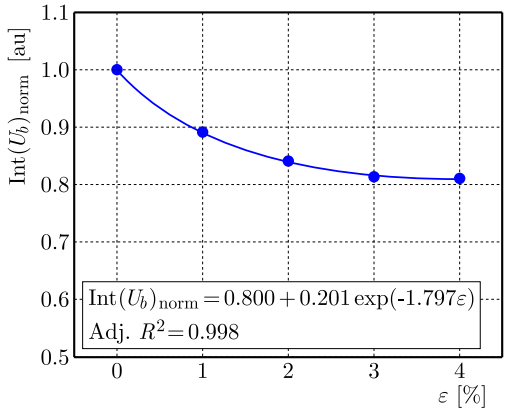

Fig. 14. Normalized BN integral versus low total axial pre-strain.

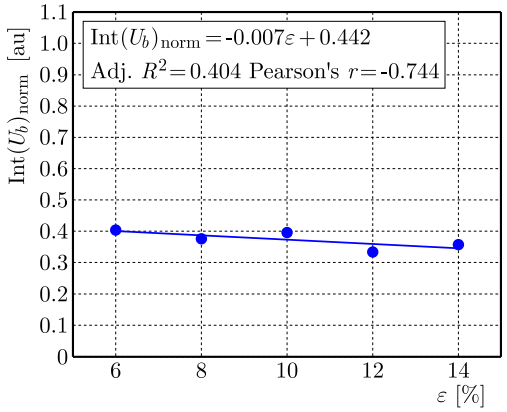

Fig. 15. Normalized BN integral versus high total axial pre-strain.

The BN signal depends strongly on dislocation density. In (Li *et al.*, 2024), the dislocation density was measured for similar medium carbon steel with martensitic structure for different levels of strain. The results were shown in the form of a dislocation density diagram versus strain (Fig. 16) (Li *et al.*, 2024).

Dislocation densities at specific strains can be calculated using the Williamson–Hall equation based on the X-ray diffraction (Deutges *et al.*, 2025): $\beta \cdot \cos(\theta) = 0.9\lambda/D + \varepsilon \cdot 2\sin(\theta)$, where θ – Bragg angle, λ – wavelength of the X-ray beam, β – full width at half maximum (FWHM) of the Bragg peaks, D – grain size, ε – lattice strain.

The term of equation $0.9\lambda/D$ is considered to be negligibly small when the effective average grain size that affects dislocation density calculations of the martensitic substructure is not smaller than 1 µm (Deutges *et al.*, 2025).

The relationship between strain and dislocation density ρ and ε can be given by the equation: $\rho = \frac{k \cdot \varepsilon^2}{b^2}$, where ε – lattice strain, b – Burger vector, k – geometrical constant ($k = 14.4$ for body-centred cubic materials) (Deutges *et al.*, 2025).

The dislocation density variations presented in Fig. 16 enable to indicate a decrease in the amplitude and integral values of the half-period BN voltage signal. Dislocation density values for the deformation range from 1 % to 4 % and are located near 21×10^{14} [1/mm^2]. However, for a strain level of 7 %, the dislocation density increases rapidly up to 26.85×10^{14} [1/mm^2]. Also, a rapid change in the amplitude and the normalized BN integral can be noticed for the strain range from 1 % to 6 %. The normalized Int(U_b) values changed from 0.81–0.89 in the 1 %–4 % strain range to 0.37–0.40 in the strain range of 4 %–6 %. The values of the BN amplitude changed from 0.31 V–0.24 V in the 1 %–4 % strain range and attained a value equal to 0.11–0.13 after pre-strain exceeding $\varepsilon = 4$ %. Thus, a sudden increase in the dislocation density causes a sharp decrease in the parameters of the BN. It was observed that the greater magnetic results diversity was obtained at the higher values of the BN amplitude. This is due to the greater sensitivity of this parameter to the microstructure features. It seems that the microstructural forms, like dislocations, change the stress levels in micro-regions of material, for example.

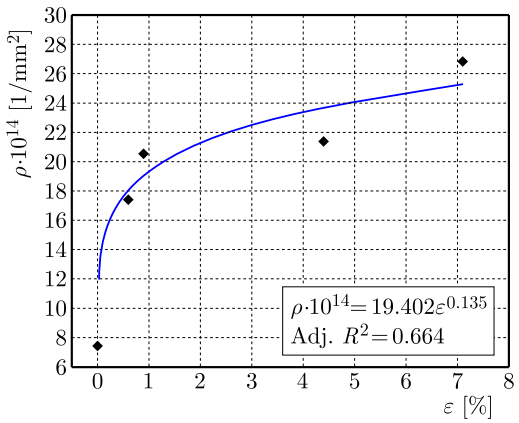

Fig. 16. Dislocation density of the martensitic medium-carbon specimens, based on (Li *et al.*, 2024).

The experimental points representing dislocation density in Fig. 16 were approximated to describe a character of dislocation density variation. In Fig. 17, the relationship between dislocation density and the normalized BN integral of the half-period voltage signal Int(U_b) was elaborated. Dislocation density values for the pre-strain levels considered in this research are included in Table 2. Figure 17 shows that the Int(U_b) related to the dislocation density of about 21×10^{14} [1/mm^2] corresponds to the deformation value equal to 2 %.

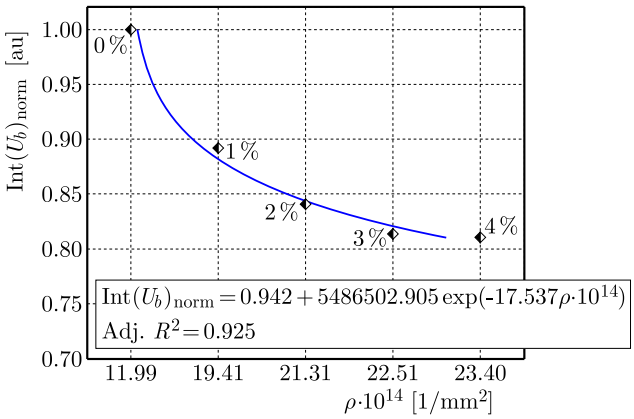

Fig. 17. Relationship between the dislocation density and normalized BN integral of the half-period voltage signal Int(U_b).

Table 2. Dislocation density values determined on the basis of approximation line from the graph in Fig. 16.

Strain level ε [%]	Dislocation density ρ [$\times 10^{14}$ 1/mm^2]
0	11.990
1	19.407
2	21.312
3	22.512
4	23.398
6	24.717

Strength and strain hardening coefficients versus the BN amplitude and integral are presented in Figs. 18–21. Both BN parameters variations, $U_{b\,pp}$ and Int(U_b), enable to identify n and K that correspond to a stress region close to the yield point. The point representing pre-strain equal to 1 % can be assigned to the elastic stress section of the tensile curve and dislocation density of about 20×10^{14} [1/mm^2]. Plastic deformation of a metal or metallic alloys begins at a stress lower than the yield strength. Plastic deformation does not occur simultaneously throughout the entire specimen volume in polycrystalline materials. A transition from the elastic stress range to the plastic one is smooth. In practice, the elastic limit is considered to be the normal stress at which the plastic deformation is still very small but measurable, from 0.001 % to 0.05 % (Dębski *et al.*, 1990). The next strain range that covers values from 2 % to 4 % is already connected with the early plastic deformation where the dislocation density is about 21×10^{14} [1/mm^2] for

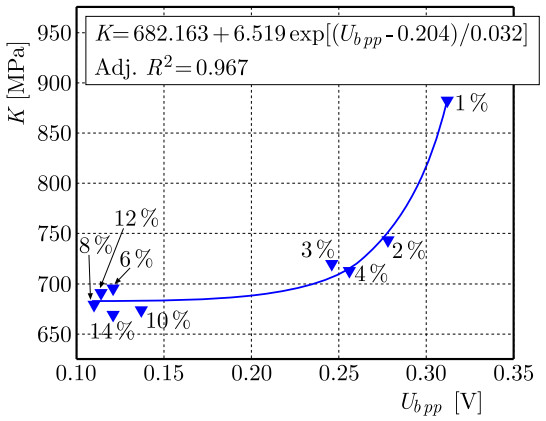

Fig. 18. Strength coefficient versus amplitude of BN.

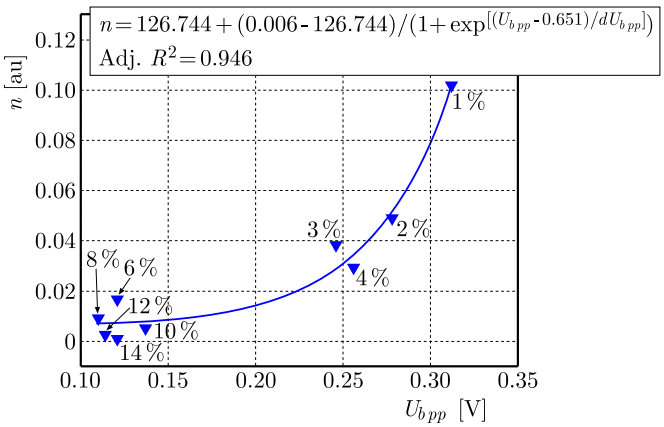

Fig. 19. Strain hardening coefficient versus amplitude of BN.

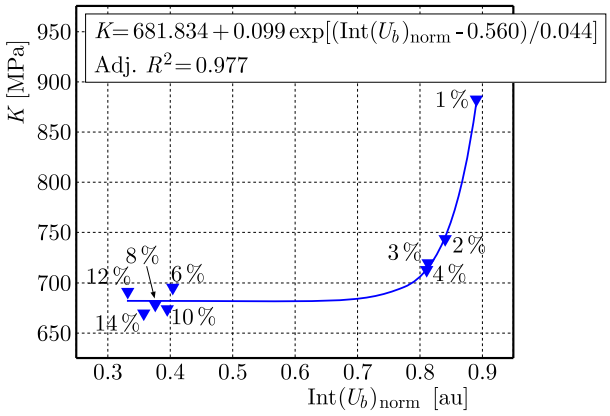

Fig. 20. Strength coefficient versus integral of BN.

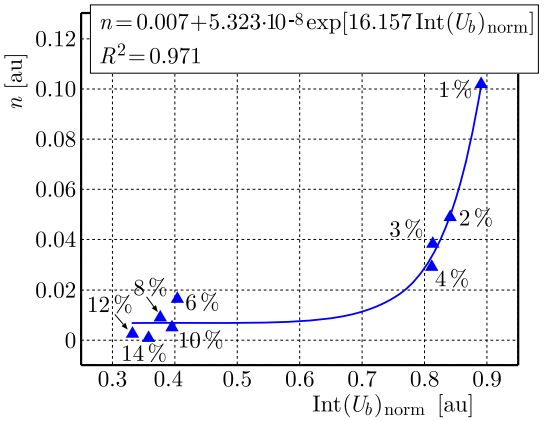

Fig. 21. Strain hardening coefficient versus integral of BN.

pre-strains equal either to 3 % or 4 %. As a consequence, both these points are next to each other on the graphs, especially in Fig. 20.

The points representing the pre-strain range from 6 % to 14 % are located close to each other on the graphs presented in Figs. 18–21 due to the insensitivity of $U_{b\,pp}$ and $\mathrm{Int}(U_b)$ parameters on the higher total pre-strain.

Figures 22 and 23 indicate that $U_{b\,pp}$ and $\mathrm{Int}(U_b)$ can be helpful in the prediction of the elastic stress and yield point of 41Cr4 after deformation in the range of 1 %–4 %. Linear relationships between the yield point/elastic limit and the amplitude/integral of the half-period voltage signal of magnetic BN were obtained in the case of low pre-strain values (Figs. 22 and 23). The pre-

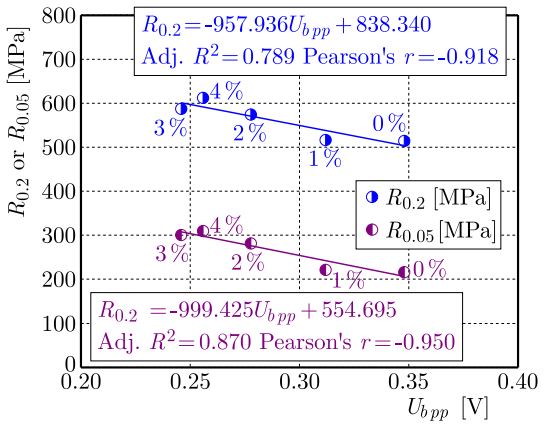

Fig. 22. Yield point and elastic limit versus amplitude of BN.

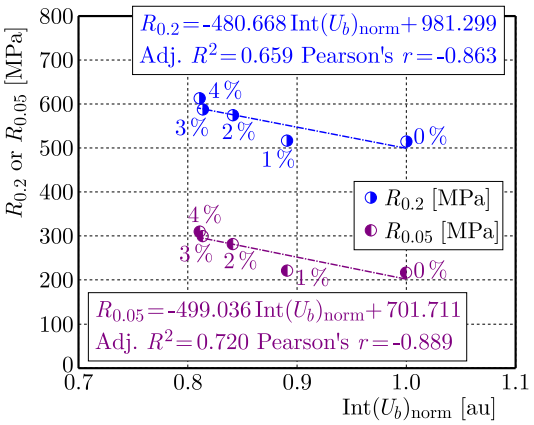

Fig. 23. Yield point and elastic limit versus integral of BN.

strain level of 1 % did not change the value of the yield point and elastic limit in comparison to the specimen before loading. On the contrary, both magnetic parameters represented a completely different character of behaviour. The changes in values of the magnetic parameters at the strain range of 1 %-–4 % are related to the material elastic region, and therefore, the stress state of 41Cr4 steel tested came back to its initial state.

5. Conclusions

Plastic deformation leads to local changes in mechanical parameters of the material tested in this study. This paper has indicated the possibility for simple identification of selected mechanical parameters of the steel subjected to prior deformation from tensile tests. This is a particularly important issue, because defects may appear during material exploitation that could change significantly its response to further loading programmes. Linear relationships were found between the stress limit/yield point and parameters determined from the BN method for low pre-strain values (0 %–4 %). The amplitude and integral of the BN were insensitive to deformations above 6 %. However, the same parameters may be successfully applied for identification of the strength and strain hardening coefficient values of ferromagnetic materials deformed up to the stress corresponding to the yield point. In conclusion, one can indicate the BN as a method that may provide effective technical support for devices inspection and structural parts diagnostics.

Acknowledgments

This work was financed by the Military University of Technology under research project 742/2004 “Modern technologies and research of modern materials used in armament technology”.

References

1. Anglada-Rivera, J., Padovese, L.R., & Capó-Sánchez, J. (2001). Magnetic Barkhausen Noise and hysteresis loop in commercial carbon steel: influence of applied tensile stress and grain size. *Journal of Magnetism and Magnetic Materials*, *231*(2–3), 299–306. https://doi.org/10.1016/S0304-8853(01)00066-X

2. Benito, J.A., Jorba, J., Manero, J.M., & Roca, A. (2005). Change of Young’s modulus of cold-deformed pure iron in a tensile test. *Metallurgical and Materials Transactions A*, *36*(12), 3317–3324. https://doi.org/10.1007/s11661-005-0006-6

3. Berdin, C., & HauŠild, P. (2002). Damage mechanisms and local approach to fracture. Part I: Ductile fracture. In I. Dloughý (Ed.), *Transferability of fracture mechanical characteristics* (pp. 167–180). NATO Science Series, vol. 78. Springer, Dordrecht. https://doi.org/10.1007/978-94-010-0608-8_12
4. Celtik, C., Ayhan, I.I., & Yurekturk, Y. (2023). Effect of double austenization and pre-annealing heat treatment on the microstructural and mechanical properties of QT 41Cr4 steel. *Transactions of the Indian Institute of Metals*, *76*(10), 2845–2855. https://doi.org/10.1007/s12666-023-02975-5
5. Cullity, B.D., & Graham, C.D. (2009). Introduction to magnetic materials (2nd ed.). Wiley-IEEE Press. https://doi.org/10.1002/9780470386323
6. Dannoshita, H., Hasegawa, H., Higuchi, S., Matsuda, H., Gong, W., Kawasaki, T., Harjo, S., & Umezawa, O. (2023). Effects of dislocation arrangement and character on the work hardening of lath martensitic steels. *Scripta Materialia*, *236*, Article 115648. https://doi.org/10.1016/j.scriptamat.2023.115648
7. Deutges, M., Barth, H.P., Chen, Y., Borchers, C., & Kirchheim, R. (2015). Hydrogen diffusivities as a measure of relative dislocation densities in palladium and increase of the density by plastic deformation in the presence of dissolved hydrogen. *Acta Materialia*, *82*, 266–274. https://doi.org/10.1016/j.actamat.2014.09.013
8. Dębski, A., Michałowski, J., Wiśniewski, S., & Wojciechowski, W. (1990). Construction materials in armament. Laboratory exercises (in Polish). Wydawnictwo Wojskowej Akademii Technicznej, Warszawa, Poland.
9. He, M., Matsumoto, T., Uchiomoto, T., Takagi, T., Chen, H., Xie, S., & Chen, Z. (2019). Caution to apply Magnetic Barkhausen Noise method to nondestructive evaluation of plastic deformation in some ferromagnetic materials. *Chinese Journal of Mechanical Engineering*, *32*, Article 104. https://doi.org/10.1186/s10033-019-0420-0
10. Hong, Y., Li, S., Li, H., Li, J., Sun, G., & Wang, Y.-D. (2018). Development of intergranular residual stress and its implication to mechanical behaviors at elevated temperatures in AL6XN austenitic stainless steel. *Metallurgical and Materials Transactions A*, *49*(8), 3237–3246. https://doi.org/10.1007/s11661-018-4655-7
11. Kashefi, M., Krause, T.W., Underhill, P.R., & Wowk, D. (2023). On the combined effect of elastic and plastic strain on Magnetic Barkhausen Noise signals. *Journal of Nondestructive Evaluation*, *42*(2), Article 55. https://doi.org/10.1007/s10921-023-00970-w
12. Kleber, X., & Vincent, A. (2004). On the role of residual internal stresses and dislocations on Barkhausen noise in plastically deformed steel. *NDT & E International*, *37*(6), 439–445. https://doi.org/10.1016/j.ndteint.2003.11.008
13. Li, J., Qiu, Y.-Y., Wang, H.-D., & Wang, Z.-X. (2019). Estimation of the strength coefficient and strain hardening exponent from monotonic tensile properties of steels. *International Journal of Steel Structures*, *19*(6), 1951–1968. https://doi.org/10.1007/s13296-019-00256-w
14. Li, J., Zhang, J.-z., Zeng, L.-y., Wang, S., Song, X.-y., Chen, N.-I., Zuo, X.-w., & Rong, Y.-h. (2024). Revealing dislocation activity modes during yielding and uniform deformation of low-temperature tempered steel by acoustic emission. *Journal of Iron and Steel Research International*, *31*(12), 3022–3036. https://doi.org/10.1007/s42243-024-01253-y
15. Makowska, K., Szymczak, T., & Kowalewski, Z.L. (2024). Fatigue behaviour of medium carbon steel assessed by the Barkhausen noise method. *Acta Mechanica et Automatica*, *18*(1), 40–47. http://doi.org/10.2478/ama-2024-0005
16. Piotrowski, L., Augustyniak, B., Chmielewski, M., & Tomáš, I. (2009). The influence of plastic deformation on the magnetoelastic properties of the CSN12021 grade steel. *Journal of Magnetism and Magnetic Materials*, *321*(15), 2331–2335. https://doi.org/10.1016/j.jmmm.2009.02.028
17. Roca, A., Villuendas, A., Mejía, I., Benito, J.A., Llorca-Isern, N., Llumà, J., & Jorba, J. (2014). Can Young's modulus of metallic alloys change with plastic deformation? *Materials Science Forum*, *783–786*, 2382–2387. https://doi.org/10.4028/www.scientific.net/MSF.783-786.2382
18. Romanowicz, P.J., Szybiński, B., & Wygoda, M. (2020). Application of DIC method in the analysis of stress concentration and plastic zone development problems. *Materials*, *13*(16), Article 3460. https://doi.org/10.3390/ma13163460

19. Rutecka, A., Kursa, M., Pietrzak, K., Kowalczyk-Gajewska, K., Makowska, K., & Wyszkowski, M. (2020). Damage evolution in AA2124/SiC metal matrix composites under tension with consecutive unloadings. *Archives of Civil and Mechanical Engineering*, *20*(4), Article 135. https://doi.org/10.1007/s43452-020-00134-x

20. Stefanita, C.-G. (1999). *Surface magnetic Barkhausen noise response to plastic yield of steel.* [Doctoral dissertation, Queen's University of Kingston], Ontario, Canada.

21. Stewart, D.M., Stevens, K.J., & Kaiser, A.B. (2004). Magnetic Barkhausen noise analysis of stress in steel. *Current Applied Physics*, *4*(2–4), 308–311. https://doi.org/10.1016/j.cap.2003.11.035

22. Stupakov, O., Pal'a, J., Tomáš, I., Bydžovský, J., & Novák, V. (2007). Investigation of magnetic response to plastic deformation of low-carbon steel. *Materials Science and Engineering: A*, *462*(1–2), 351–354. https://doi.org/10.1016/j.msea.2006.02.475

23. Vaidyanathan, S., Moorthy, V., Kalyanasundaram, P., Jayakumar, T., & Raj Baldev (1999). Effect of different stages of tensile deformation on micromagnetic parameters in high-strength, low-alloy steel. *Metallurgical and Materials Transactions A*, *30*(8), 2067–2072. https://doi.org/10.1007/s11661-999-0017-9

24. Wang, X., Chen, J.-G., Su, G.-F., Li, H.-Y., & Wang, C. (2020). Plastic damage evolution in structural steel and its non-destructive evaluation. *Journal of Materials Research and Technology*, *9*(2), 1189–1199. https://doi.org/10.1016/j.jmrt.2019.11.046

25. Yamaguchi, K., Adachi, H., & Takakura, N. (1998). Effects of plastic strain and strain path on Young's modulus of sheet metals. *Metals and Materials*, *4*(3), 420–425. https://doi.org/10.1007/BF03187802

Manuscript received December 20, 2024; accepted for publication May 14, 2025; published online July 19, 2025.